

Fracture Toughness of MDF and other Materials with Fiber Bridging

Noah Matsumoto and John A. Nairn*

ABSTRACT

We measured the fracture toughness of MDF panels with two different densities by using crack propagation experiments and energy-based fracture mechanics. The two challenges were to identify the energy associated with crack propagation and to measure actual crack lengths. Fracture energy calculations needed to account for crack-plane interference effects. Crack growth detection required digital image correlation (DIC) methods. The toughness of MDF depended on density and varied from $G_c = 2650 \text{ J/m}^2$ for lower density to $G_c = 5680 \text{ J/m}^2$ for higher density. By comparison of MDF experiments to prior experiments on unidirectional carbon fiber/polysulfone composites, neat polysulfone polymer, and Corian[®] sheet product, particulate-filled composites, we derived a general scheme for fracture characterization of composites. The standard fracture mechanics methods in ASTM E399 are invalid for certain types of composite cracking processes. For these materials, ASTM methods can be replaced by energy methods. The key experiments needed to determine when ASTM E399 is invalid and which energy methods are appropriate are described.

INTRODUCTION

The composite literature has occasionally seen (misguided) reports that fracture mechanics does not apply to composites. Using a general definition of fracture mechanics that it is the engineering discipline of predicting when the dominant flaw in an object will get larger [1], fracture mechanics always applies to composites (*i.e.*, “by definition”). Where literature reports claim that fracture mechanics does not work, the problem can usually be traced to methods extracted from fracture mechanics standards but applied inappropriately to composite materials that violate the assumptions of that method.

For example, ASTM E399 [2] outlines a standard procedure for measurement of plane-strain fracture toughness using a stress intensity factor approach. This method, however, is based on several assumptions about the material and about the crack propagation process. A subtle assumption, often unrecognized, is an assumption that fracture proceeds by *self-similar* crack propagation. This assumption not only means

* Wood Science & Engineering, Oregon State University, Corvallis, Oregon 97331-5751, USA.
Contact: John.Nairn@oregonstate.edu

the crack propagates straight, but also means the crack-tip stress region of an extended crack is indistinguishable from the initial crack, except for factors involving crack length. For example, a common fracture process in fiber-reinforced composites, and in natural materials such as wood, is to have fibers bridging across the crack plane. Since the extended crack has fiber bridging while the initial crack does not, this type of fracture is not self-similar crack propagation. Thus, an observation of fiber bridging invalidates an ASTM E399 approach, but it does not invalidate fracture mechanics. The task with composites is to use appropriate analysis methods. Since many composite materials are approximately linear elastic, several methods are available. In general the preferred approaches are based on energy release rate rather than stress intensity factor [3].

This paper illustrates fracture mechanics of composites by presenting several types of possible fracture processes and the appropriate analysis tools for each one. The most challenging material was medium density fiber board (MDF, a wood-based composite with fine wood fibers bound together with a small amount of polymeric glue [4]). This material exhibited fiber bridging and complicated crack growth. The complicated crack growth precluded several energy methods and made it difficult to measure crack length. By accounting for crack-plane effects and developing new methods to measure crack length, it was possible to measure *true* toughness of MDF. A second composite example was a unidirectional, fiber-reinforced polymer. Like MDF, this material had fiber bridging, but had fewer of the crack growth complications. This material could be analyzed by the techniques used for MDF, but could also be analyzed by simpler methods not available for MDF. The last two examples were a particle-reinforced composite and a neat polymer. These two materials had no fiber bridging and had essentially self-similar crack propagation. These materials could be analyzed by all methods including standard ASTM E399 stress intensity factor methods.

The various methods described here encompass nearly any material type in which nominally straight crack propagation occurs from a dominant crack. This paper includes a scheme for categorizing key features during crack propagation that determine the type of analysis method needed for correctly measuring fracture toughness.

MATERIALS AND METHODS

Materials

The medium density fiber boards (MDF panels) were provided by Flakeboard, Springfield, Oregon, USA at two levels of density — 0.609 g/cm³ (38 lbs/ft³) and 0.769 g/cm³ (48 lbs/ft³). The 4 ft X 8 ft panels were cut into four 2 ft X 4 ft panels with two of them having the long axis of the full panel in their 4 ft direction while the other two had the transverse axis of the full panel in their 4 ft direction. Due to the highly hygroscopic nature of natural wood, each specimen was conditioned in a room at 20°C

and 65% relative humidity until equilibrium prior to testing. Periodic measurements of the specimens' weights were made and equilibrium was confirmed by stabilization of the weights.

The carbon fiber/polymer composites used Hercules AS-4 carbon fiber in Union Carbide UDEL P1700 polysulfone (PSF) matrix (now manufactured by Solvay Advanced Polymers). The 12-ply, unidirectional laminates were manufactured by duPont; the details are given in Ref. [5]. The neat polysulfone (PSF) matrix was Union Carbide UDEL P1700 polysulfone purchased from Westlake Plastics as 1.59 mm thick extruded sheet [5].

The Corian[®] sheet product, which is polymethyl-methacrylate highly filled with inorganic material, was provided by the duPont company. Note that this Corian[®] sheet product and the experiments were done in 1984. Current Corian[®] sheet product is nominally the same, but may differ (*e.g.*, in amount and type of inorganic filler) from the material in this paper.

Experiments

All fracture experiments were done with analogs of the ASTM E399 [2] compact tension specimen illustrated in Fig. 1. Most specimen features scale with the crack line width, W . The crack length, a , is measured from the crack tip to the center of the pin-loading holes. The standard ASTM specimen has $\Delta = 0$; some experiments here extended the specimen to allow for extra crack propagation.

The MDF specimens were cut with $W = 76.2$ mm (3 in) and $\Delta = 31.75$ mm (1.25 in) with the crack propagation direction in the longitudinal direction of the panel. Although MDF panels are approximately isotropic, care was taken to always orient crack growth in the longitudinal direction. Results in the transverse direction will be reported elsewhere. All MDF specimens had thickness $B = 12.7$ mm (0.5 in). Crack tips and notches were made using a table saw with a specially ground carbide-tipped blade that produced a 45 degree angle at the crack tip.

The unidirectional laminate specimens used $W = 25.4$ mm (1 in) and $\Delta = 0$. The average laminate thickness was $B = 1.60$ mm. The crack was cut parallel to the fiber direction using a diamond blade. The neat PSF specimens also used $W = 25.4$ mm (1 in) and $\Delta = 0$ and had average thickness of $B = 1.59$ mm. The crack was cut with a band saw and sharpened with a razor blade prior to the test.

The Corian[®] sheet product specimens used $W = 50.8$ mm (2 in) and $\Delta = 0$, and had average thickness of $B = 18.7$ mm. The crack notch was machined with a 45° crack tip and was sharpened with a razor blade prior to testing.

All specimens were subject to crack propagation experiments. The specimens were loaded using standard mechanical testing frames and loaded at 0.5 mm/min. Data was collected for load and crosshead deflection. For improved accuracy in the MDF experiments, an Epsilon[®] clip style extensometer was fixed at two pins inserted into the MDF near the loading pins. All MDF displacement results came from the extensometer readings. The loading was continued until the crack approached the right

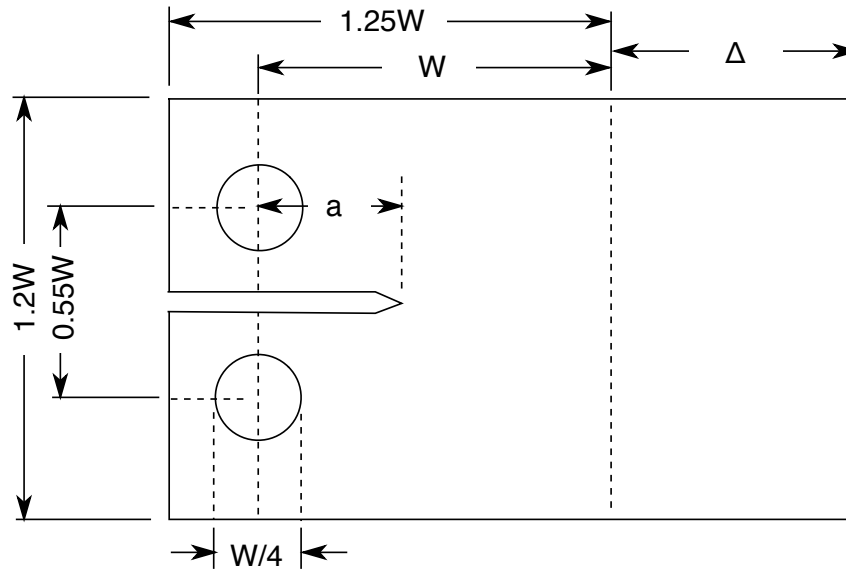


Figure 1: Compact-tension style specimen used for all experiments. The sample scales with crack line width W . A specimen with $\Delta = 0$ is a standard compact tension specimen. Some specimens had nonzero Δ to provide more specimen for larger amounts of crack propagation. The machined-in crack plane had a nominal width of $W/16$.

edge of the specimen. In many experiments, the loading was periodically stopped and fully or partially unloaded. While unloaded, the new crack length was recorded. Upon reloading the new specimen compliance, which depends on crack length, was recorded from the slope of the load-deflection curve. In MDF panels, unloading was suspected to influence the result (see below). For these specimens the displacement was monotonically increased and the crack growth during propagation was recorded as described below.

A key experimental result for analysis of crack propagation experiments is the crack length during the experiments. For neat PSF and Corian[®] sheet product, the crack propagation could easily be observed on the specimen surface. The crack length was measured using a Gaertner traveling microscope. The crack length for unidirectional laminates was observed by painting the sample with white out. A crack through the brittle white paint on the black carbon-fiber laminate could easily be observed in the traveling microscope.

Crack length in the MDF panels was difficult to observe. As the crack propagated, effects of the crack are apparent on the surface, but the actual position of the crack tip was unclear. To solve this problem, we used digital image correlation (DIC) methods [6,7] to measure the strain field ahead of the crack tip. In brief, two digital cameras were positioned approximately 1.5 ft from the specimen loading position and carefully focused. The aperture of each camera was adjusted such that intensity of light entering each camera was roughly equal. The image correlating software, VIC-3D[®], was then calibrated by correlating images of a calibration target placed a various positions in the viewing area. The square target was white with black dots equally spaced apart in a

square pattern whose dimensions took up approximately one fourth of the pixel area of the captured images. The roughly 25 calibration images were taken with the Correlated Solutions® image acquisition software, VIC Snap®, and covered every point in the viewing area including, in front of, and behind the focal plane of the cameras. Once the VIC-3D® software was calibrated, the testing specimens were placed in the loading machine for image capturing during experimentation. VIC Snap® was set to take one picture per second during testing. A signal from the testing frame was input to the software to enable synchronization of the captured images with the load-deflection results.

Analysis of images at successive loads through image correlation allows one to map the deformation field [6,7]. Differentiation of the deformation field results in calculation of any component of strain. Figure 2 shows strain in the loading direction as a function of position along the uncracked portion of the specimen for a series of increasing crack lengths. The strain was high near the crack tip and decreased as a function of distance from the crack tip. It was not possible to assign an absolute crack tip location from such results because of artifacts that occur very close to the crack tip. Relative amounts of crack growth, however, could accurately be determined by the shift between curves at two crack lengths (*e.g.*, see Δa in Fig. 2). We thus measured the initial crack length and then determined subsequent crack lengths from incremental amounts of crack growth between successive strain profiles throughout the experiment.

Energy Methods

The left side of Fig. 3 shows load-displacement results for elastic fracture where the test is periodically unloaded after increments in crack growth. The unloading (or reloading) curve at each new crack length defines the compliance as function of crack length, $C(a)$; the point at which the crack starts propagating (the peak load) defines the failure load, $P(a)$, and failure displacement, $u(a)$, for fracture, each as a function of crack length. The right side of Fig. 3 shows a single loading and unloading envelop with two possible unloading curves. One unloading curve (segment CA) returns to the origin while the other curve (segment CD) returns to a residual displacement, u_R , after unloading. In crack propagation experiments with discrete results at successive crack lengths, the key results will be failure load, P_i , failure displacement, u_i , crack length, a_i , and compliance, C_i (from slope of load-deflection curve), as labeled in Fig. 3. Subscript i is for results at crack length a_i while subscript j is for results at the new longer crack length a_j .

During elastic fracture, if the unloading curve returns to the original origin, the fracture energy is the area within the triangular area ABC. The fracture toughness is the energy per unit fracture area. The toughness from a discrete observation of crack growth, $\Delta a = a_j - a_i$, can be calculated various ways. Two convenient methods are:

$$G_c = \frac{P_i P_j (C_j - C_i)}{2B \Delta a} \quad (1)$$

and

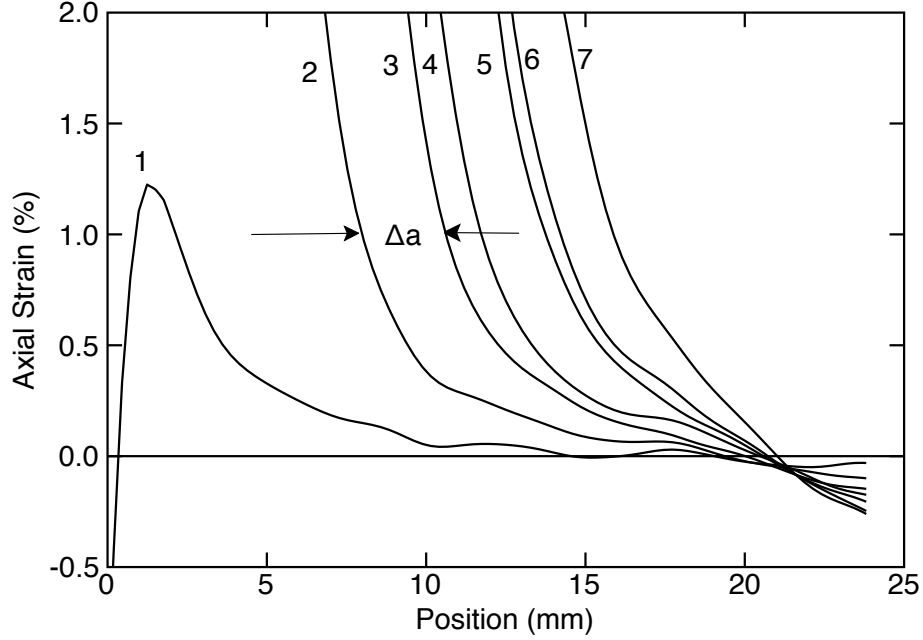


Figure 2: Axial strain as a function of position along the crack line (see Fig. 1) for specimens with increasing crack lengths as measured by digital image correlation (DIC). The shift between any two curves is a measure of crack growth.

$$G_c = \frac{P_i(u_j - u_0) - P_j(u_i - u_0)}{2B\Delta a} \quad (2)$$

Both equations assume an ideal triangular area ABC. The first is based on measured loading and unloading compliances (and C_j comes from segment CA); the second is based instead on measured displacements at key points. For continuous crack propagation experiments, a single specimen will provide multiple results at different crack lengths. A discrete fracture toughness can be calculated from any pair of points, i and j , on the same specimen.

In the limit of small crack growth, the result in Eq. (1) reduces to the well-known linear elastic fracture mechanics result [3] of

$$G_c = \frac{P^2}{2B} \frac{dC}{da} \quad (3)$$

One way to use this equation is to fit experimental results for compliance, C_i , as function of crack length, a_i , differentiate the fit to find dC/da , and finally substitute that result along with a fit result for load as a function of crack length, $P(a)$, into Eq. (3) to find toughness as a function of crack length. This compliance-calibration method was used for some experiments. The compliance and load were fit to fourth-order polynomials based on observations that theoretical dC/da can be fit to third- or fourth-order polynomials [2].

If the unloading curve does not return to the origin, a new analysis is needed, but the analysis method depends on the reason the crack did not return to the origin. Three

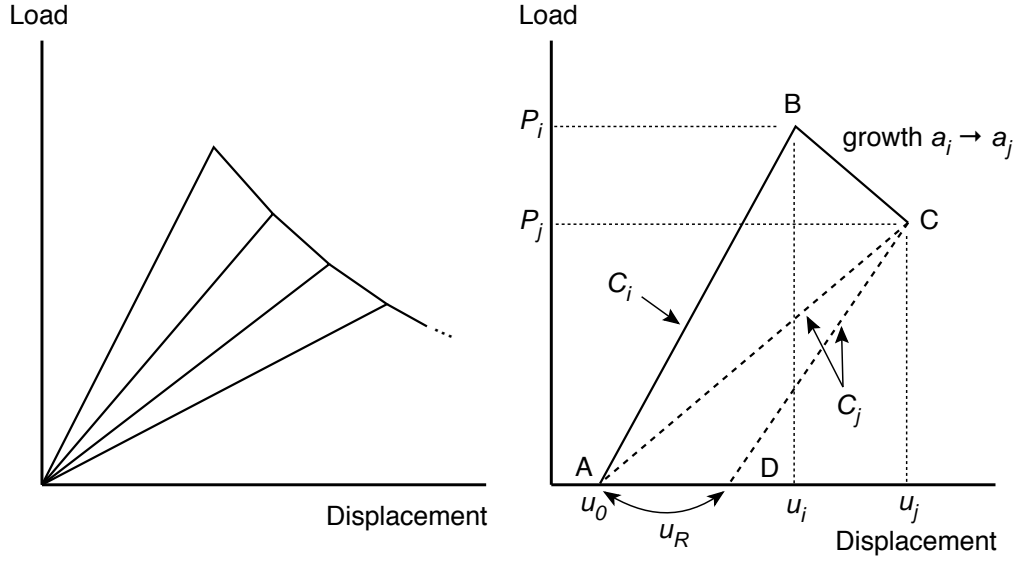


Figure 3: Left side is stress strain curve with loading and unloading at successive crack lengths and assuming elastic fracture with the unloading returning to the origin. The right side shows a single loading and loading envelop that may return to the origin along segment CA or to a residual displacement along segment CD. The compliance C_i comes from the slope of the loading curve. The compliance C_j comes from slope of one of the two unloading (or reloading) curves.

possibilities are residual stresses, plastic energy dissipated during fracture, or crack-plane interference effects that impede the unloading process [3]. If the reason is residual stresses, the energy analysis has to be modified to account for residual stress effects [3,8]. Residual stresses will change the origin only if the two halves of the specimen being separated by crack growth have residual stresses that induce curvature or distortion of those sections. For example, origin-altering, residual stresses in double cantilever beam specimens are only present if the delaminated arms are not symmetric laminates and therefore curve due to residual stresses [8]. Since none of the specimens tested here had such asymmetries, residual stress effects were ruled out.

If the unloading curve is shifted due to plasticity effects, the problem becomes an elastic-plastic fracture mechanics problem [1,3]. Although there is debate about the preferred analysis of elastic-plastic fracture, one approach is to include the entire area in the ABCD quadrilateral. This area can be found by integrating experimental results for loading and unloading. Alternatively, from discrete experimental results

$$G_c = \frac{C_i P_i^2 + (P_i + P_j)(u_j - u_i) - C_j P_j^2}{2B\Delta a} \quad (4)$$

where C_j now comes from segment CD. In the limit of small crack growth, Eq. (4) reduces to

$$G_c = \frac{P^2}{2B} \frac{dC}{da} + \frac{P}{B} \frac{du_R}{da} \quad (5)$$

where u_R is the residual displacement remaining after unloading [3].

The third alternative is that something in the crack plane inhibits the two crack faces from coming back together. For example, during MDF fracture the crack plane is bridged by wood fibers that have been partially removed from the crack surfaces. Because these fibers cannot slide back into the surface, crushing of the fibers inhibits unloading making it look stiffer than if that crack-plane interference had been absent. Any energy associated with crack-plane interference is not part of the fracture process and therefore should not be included in the fracture toughness. The total energy in the ABCD quadrilateral needs to be partitioned into energy associated with fracture and energy associated with crack-plane interference upon unloading. If the fracture can be characterized as consisting mostly of elastic processes, a logical partitioning is to consider the ABC triangle as the fracture energy and the ACD triangle as the crack-plane interference energy. The key experiment for identifying crack-plane interference is to monotonically load to some crack length, remove the crack-plane process zone (such as cutting it out with a saw), and then to unload [3]. If the unloaded specimen returns to the original origin, the fracture can be identified as elastic with toughness given by the ABC triangle. If the unloaded specimen does not return to the origin, then the fracture process itself caused permanent deformation and the toughness should include the entire ABCD quadrilateral area [3].

In the case of elastic fracture with crack-plane interference, any unloading might alter the crack process zone and change the results. The crack propagation experiments therefore have to be done with monotonic loading, meaning they cannot include the unloading steps that are required to monitor compliance as a function of crack length. For such data, the toughness can be calculated only from Eq. (2). The methods that depend on measured compliance (e.g., Eqs. (1) and (3)) cannot be used.

Stress Intensity Factor

An alternate approach to fracture testing, as described in ASTM-E399 [2], is to calculate the stress intensity factor at failure. When using a standard compact tension specimen (see Fig. 1 but with $\Delta = 0$), one measures the crack length and failure load and finds the critical stress intensity factor, K_c , using

$$K_c = \frac{PY(a/W)}{BW} \sqrt{a} \quad (6)$$

where $Y(a/W)$ as a calibration function that is given by a fit to numerical results using

$$Y(x) = \frac{2+x}{x^{1/2}(1-x)^{3/2}} (0.886 + 4.64x - 13.32x^2 + 14.72x^3 - 5.6x^4) \quad (7)$$

where $x = a/W$. Note that the ASTM approach assumes the fracture proceeds by self-similar crack growth and further that self-similar crack growth implies a straight crack with stress-free fracture surfaces and no evolving fracture process zone.

Because energy release rate and stress intensity factor are related by

$$K_c = \sqrt{G_c E_{eff}} \quad (8)$$

where E_{eff} is an effective modulus depending on crack tip stress state (*e.g.*, plane stress vs. plane strain [1,3]), and because for elastic fracture in the absence of residual stress effects, G_c is given by Eq. (3), it is easy to derive

$$\frac{1}{C_0} \frac{dC}{d(a/W)} = 2aY^2(a/W) \quad (9)$$

where $C_0 = 1/(BE_{eff}W)$. Because $Y(a/W)$ is a material-independent calibration function, Eq. (9) implies that the normalized variation in compliance with crack length is also a material-independent quantity. Conversely, if experiments show that compliance does not vary as predicted by $Y(a/W)$, those experiments demonstrate that the stress intensity approach will be an invalid approach to fracture for that material. Because energy methods do not depend on any assumed crack process, they can be used for any material provided the energy and crack length are correctly measured and provided the measured energy is correctly identified with fracture work and not with alternative mechanisms such as crack-plane interference effects.

RESULTS

MDF Toughness

Figure 4 shows initial experiments on MDF for crack propagation done with periodic loading and unloading at several crack lengths. Clearly the unloading stages did not return to the original origin. Instead, as illustrated by segment CD in Fig. 3, a residual displacement developed. To test if the residual displacements were caused by crack-plane interference, a sample was loaded to some crack length and held. The crack process zone was removed from the specimen with a saw and then the load was decreased to zero. A comparison of this specimen to a specimen where the process zone was not removed is in Fig. 5. The solid line is for the specimen with the zone removed. The load dropped during the removal process (dashed vertical line), but when unloaded, it returned fairly close to the origin. This experiment is evidence that MDF fracture is nearly elastic, but that it has crack-plane interference. The dashed curve is the second loading and unloading envelop for a sample without removing the process zone. For better comparison, this data was normalized to the other data by matching peak load and loading compliance. The initially steep slope was caused by the crack-plane effects arising for the first unloading step; the effective origin of the dashed curve is assumed to be extrapolation of the linear loading region back to zero load, which would be near 0.0 mm in Fig. 5. Upon unloading, this specimen was stiffened by fracture debris in the crack plane area. Because of the stiffening, the unloading resulted in a residual displacement of about 0.5 mm.

Our hypothesis was that MDF fracture is elastic, but develops crack-plane interference. As a consequence, it was not possible to include unloading in the experiment. The unloading would result in extra energy crushing the crack-plane material and could change the process zone thereby altering the toughness. For such a material, one cannot use any method that relies on measurement of compliance (*e.g.*,

Eqs. (1) or (3)). It would also be an error to unload and measure the entire area under the curve (Eqs. (4) or (5)). Finally, the fiber bridging invalidates the stress intensity approach (Eq. (6)). The only remaining option is Eq. (2). The process was to monotonically load a specimen to induce continuous crack propagation. Periodically during the experiment, we would record load, P_i , displacement, u_i , and take a picture for use in DIC methods to find crack growth since the last image, Δa . These data are sufficient for calculation of G_c using Eq. (2). This equation extrapolates from each pair of (P_i, u_i) points back to the initial displacement at u_0 to find the triangular area (e.g., area ABC in Fig. 3). By our hypothesis, this area represents the actual energy released during crack growth. To get extra crack propagation, these continuous experiments extended the compact tension specimen using extra length of $\Delta = 31.75$ mm. The main reason to use the standard shaped compact tension specimen is for use with the specimen-dependent calibration function in Eq. (7). Since the stress intensity approach cannot be used for MDF, there was no incentive to retain the standard compact tension geometry. The energy method directly measures energy without need for specimen-dependent corrections.

Toughness results for two lower-density specimens (0.609 g/cm^3 or 38 lbs/ft^3) and one higher density specimen (0.769 g/cm^3 or 48 lbs/ft^3) are plotted in Fig. 6. For all specimens, the first few points tended to be lower. We expect the first points are prior to development of crack bridging and therefore naturally have a lower toughness. After about 10-15 mm of crack growth, the toughness leveled off, albeit with some scatter. The average value of this plateau region can be taken as the toughness. At very long

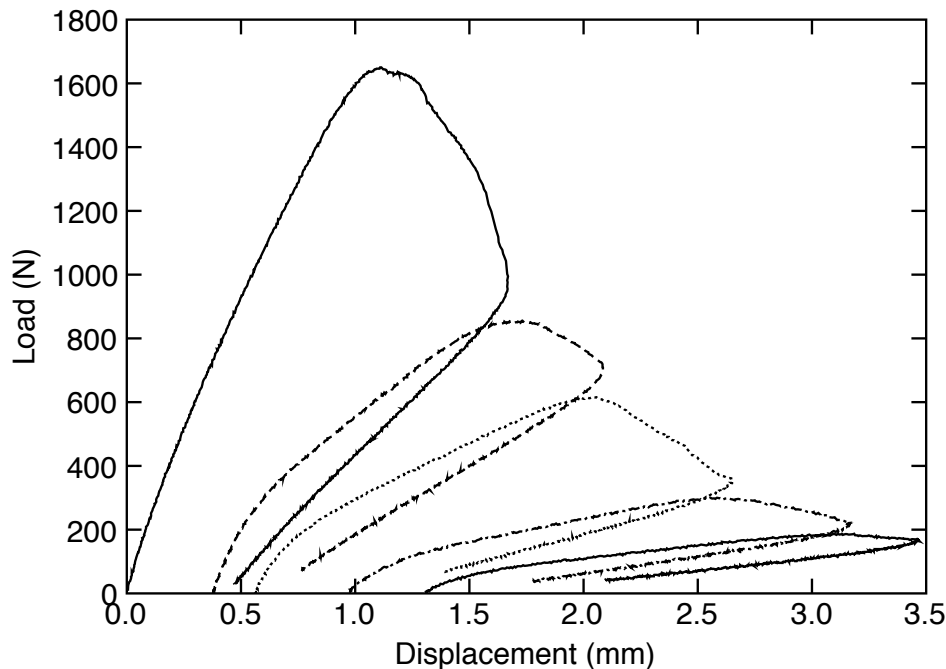


Figure 4: Load deflection curve for a typical MDF specimen. As the crack propagated, the specimen was periodically unloaded and then reloaded to continue propagation.

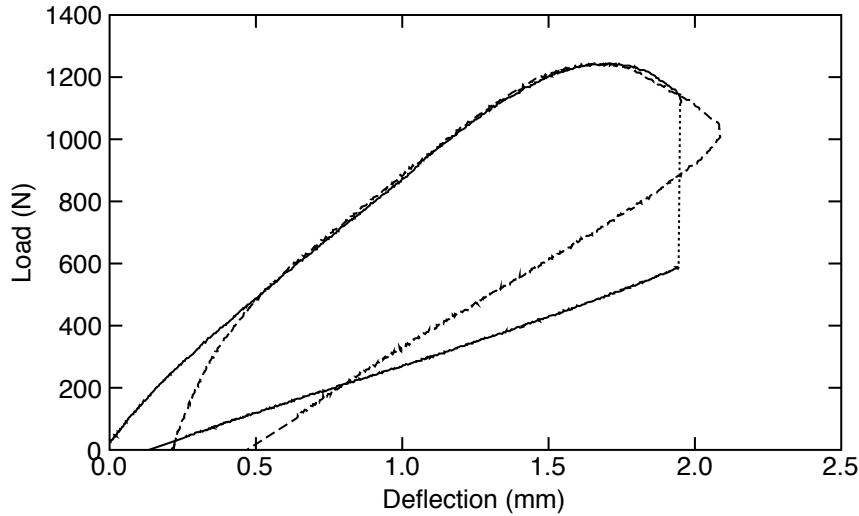


Figure 5: The dashed line is the second loading and unloading envelop of the specimen in Fig. 4. The solid line is a new specimen that was loaded, had the crack process zone removed from the sample, and then unloaded. The dashed portion of the solid curve is the load drop occurred while removing the process zone.

crack lengths, some toughness results, especially for lower density panels, got very high. We attributed these results to edge effects and ignored those points in the averaging. The average toughness (for crack growth between 15 and 45 mm) for the lower density specimens (0.609 g/cm^3 or 38 lbs/ft^3) was 2650 J/m^2 and for the higher density specimens (0.769 g/cm^3 or 48 lbs/ft^3) was 5680 J/m^2 .

Unidirectional Composite Toughness

Like MDF fracture, crack growth parallel to the fibers in a unidirectional carbon fiber/PSF composite has fiber bridging. Unlike MDF, however, the fibers are aligned and thus when unloaded, less crack-plane interference occurred. The experimental finding was that unloading nearly returned to the origin. The toughness for such an elastic material, with little or no crack-plane interference, can be found from the triangular area using any of Eqs. (1)-(3).

Figure 7 gives results of calculating G_c using discrete data from five specimens for load, P_i , compliance, C_i , and crack length, a_i , and substituting into Eq. (1). These results are a reanalysis of data from Ref. [5]. As with MDF, fiber bridging caused the first few points to be lower until the bridging zone developed at a/W of about 0.5. Also similar to MDF, the points at very long crack lengths were high, which was attributed to edge effects. A toughness of $G_c = 305 \text{ J/m}^2$ was found by averaging the plateau region for a/W between 0.5 and 0.75.

Since we had results for load and crack length (P_i and a_i), it was simple to substitute into Eq. (6) and calculate an apparent stress intensity factor, K_c . As expected, the results did not give a good fracture mechanics result. The apparent K_c increased steadily with crack length from $2 \text{ MPa } \sqrt{\text{m}}$ to $16 \text{ MPa } \sqrt{\text{m}}$. The cause of the increase

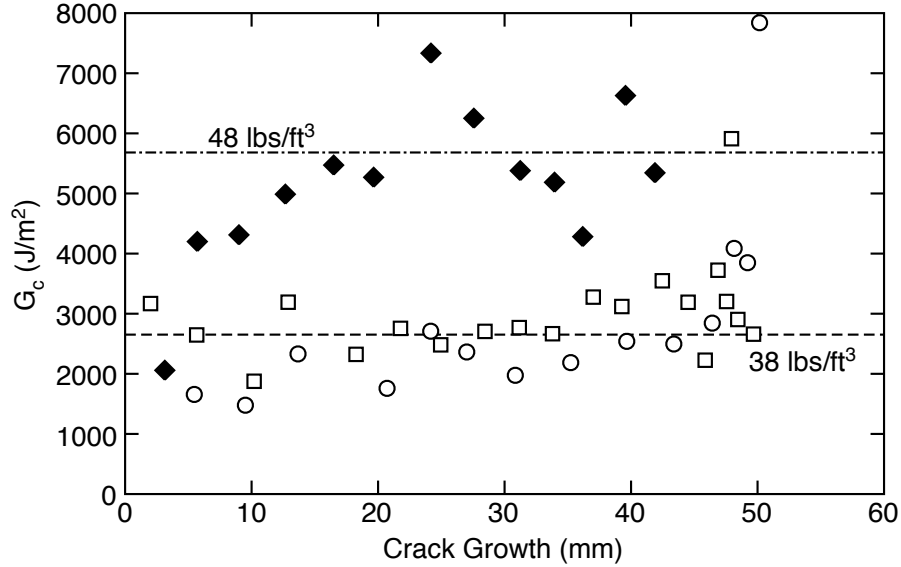


Figure 6: Toughness of lower-density MDF (38 lbs/ft³) and higher-density MDF (48 lbs/ft³). The toughness was found using Eq. (2) for continuously loaded specimens. The dashed lines are averages over the plateau regions between 15 mm and 45 mm of crack growth.

was fiber bridging. Since the stress intensity approach assumes no fiber bridging, it gives an invalid result for toughness.

Figure 8 shows a compliance calibration procedure where the results from the five specimens were combined and fit to fourth-order polynomials to find $P(a)$ and $C(a)$. The fit results were substituted into Eq. (3) to find a continuous calculation of $G_c(a)$. The results were similar to the discrete calculation showing an initial increase followed by a plateau and ending in an increase due to edge effects. A toughness of $G_c = 275$ J/m² was calculated from the plateau region (a/W from 0.5 to 0.75); it is close to the plateau average of the discrete analysis in Fig. 7. The continuous $G_c(a)$ curve is also plotted with the discrete analysis in Fig. 7 showing that the two methods are consistent.

To probe fiber bridging effects, identical experiments were run on the neat PSF matrix; since there were no fibers, there could be no fiber bridging. The results are summarized in Fig. 9. For this type of material, the toughness can be found by any method discussed above. The open symbols are calculation of G_c using discrete data from three specimens and Eq. (1). The dotted curve is the compliance calibration procedure from the same data using fit results for $P(a)$ and $C(a)$ substituted into Eq. (3). The plateau region of the fit method goes through the discrete data analysis; the toughness averaged over the plateau region was $G_c = 1550$ J/m². The critical stress intensity factor approach using Eq. (6) was also valid; the results are the filled symbols in Fig. 9. The average toughness was $K_c = 2.55$ MPa \sqrt{m} .

By Eq. (8), the modulus can be calculated from G_c and K_c ; the result is $E_{eff} = 4195$ MPa. This modulus is higher than the measured result for UDEL 1700 polysulfone of 2480 MPa [9], but it is not unreasonable. ASTM E399 states that the test is not a plane-strain toughness unless the specimen thickness, B , satisfies:

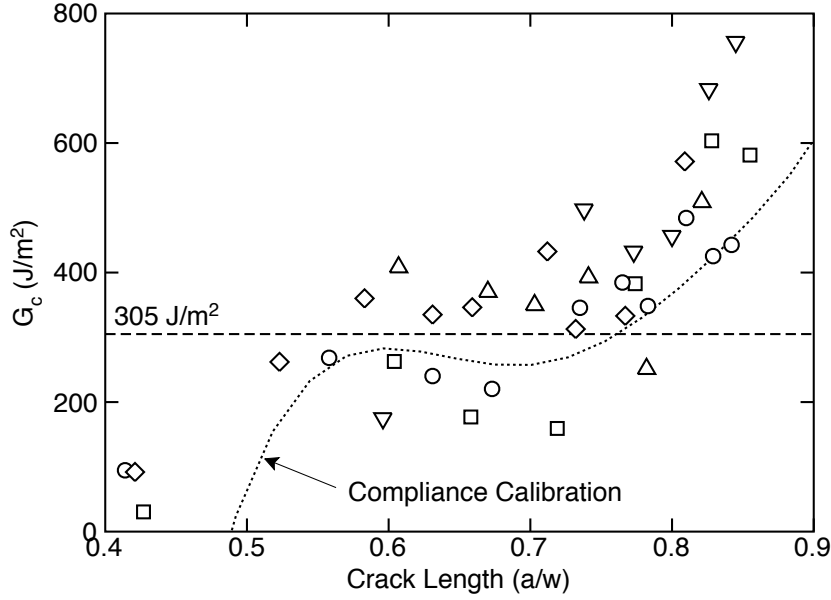


Figure 7: Discrete calculation of toughness for a 12-ply, unidirectional carbon fiber/PSF composite. The dashed line is an average of the plateau region for a/W between 0.5 and 0.75. Each symbol type is one of the five specimens. The dotted line is calculation of G_c using the compliance calibration method as explained in the text.

$$B \geq 2.5 \left(\frac{K_c}{\sigma_y} \right)^2 \quad (10)$$

From the measured toughness above and yield strength of 70 MPa [9], the thickness requirement for plane-strain toughness is $B \geq 3.3$ mm. The test is not a valid plane-strain toughness. Nevertheless, the energy methods and the stress intensity approach still measure the *true* toughness for this specimen. The values might change for thicker specimens, but the analysis methods would be the same.

Corian Composite

The last example is Corian[®] sheet product. Unlike neat PSF, this material is a composite. Unlike MDF or unidirectional composites, this composite has no fibers and thus should not be affected by fiber bridging. The results are summarized in Fig. 10. The toughness for Corian[®] sheet product could be found by any method discussed above. The open symbols are calculation of G_c using discrete data from three specimens and Eq. (1). The dotted curve is the compliance calibration procedure from the same data using fit results for $P(a)$ and $C(a)$ substituted into Eq. (3). The plateau region of the fit method goes through the discrete data analysis; the toughness averaged over the plateau region was $G_c = 207$ J/m². The critical stress intensity factor approach using Eq. (6) was also valid; the results are the filled symbols in Fig. 10. The average toughness was $K_c = 1.39$ MPa $\sqrt{\text{m}}$.

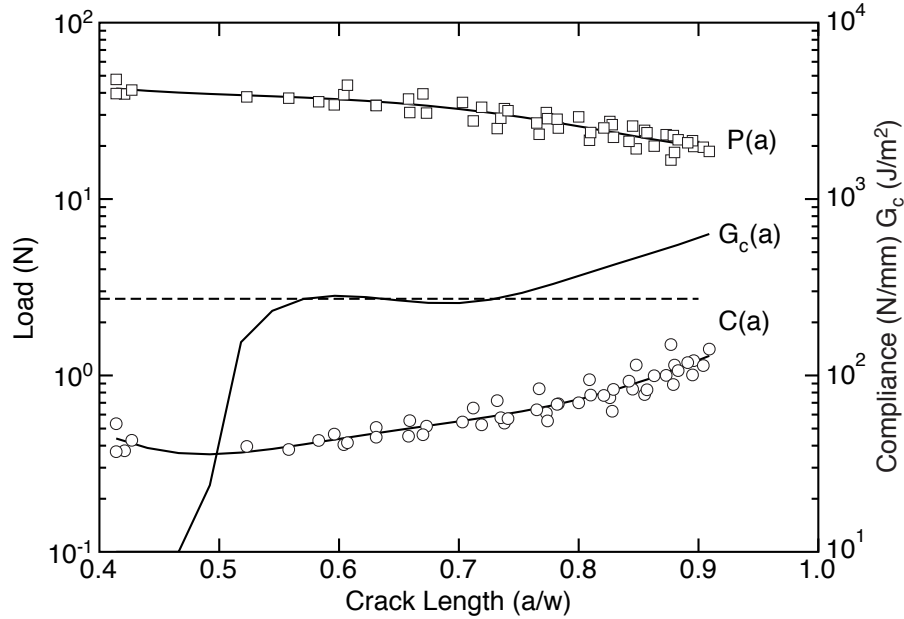


Figure 8: A compliance calibration analysis for carbon fiber / PSF unidirectional composites. The symbols are experimental results for propagation load, $P(a)$, and compliance, $C(a)$, from five specimens. The lines through the experimental results are fourth order polynomial fits to the data. The line labeled $G_c(a)$ was calculated from the data fits using Eq. (3). The dashed line is the average toughness of 275 J/m^2 over the plateau region of the calculated curve (a/W from 0.5 to 0.75).

The modulus calculated from Eq. (8) using G_c and K_c was $E_{eff} = 9330 \text{ MPa}$; this result was essentially identical to the measured modulus of 9650 MPa . By Eq. (10), and using the measured yield strength of Corian[®] sheet product of 41 MPa , the thickness require for plane-strain conditions was $B \geq 2.9 \text{ mm}$. Since this thickness is much less than the specimen thickness (18.7 mm), the experiments provided valid plane-strain toughness for Corian[®] sheet product.

DISCUSSION

These results for two types of fiber-reinforced composites, a particulate reinforced composite, and a neat polymer provide examples of different methods required to measure toughness of composites. We can outline a procedure that should produce valid results for fracture testing of any predominantly elastic material in which crack propagation can be observed and is nominally straight.

The first test should be to load until there is crack propagation and then unload. If the unloading returns to near the origin of original loading, then crack-plane interference or similar effects can be ignored. Any such material can be studied using Eqs. (1) to (3). Eqs. (1) and (3) require measurement of compliance as a function of crack length. Thus the crack propagation must be periodically interrupted and unloaded to measure it. Eq. (2) can be done without compliance experiments, but requires continuous monitoring of crack length as a function of load. In some materials, crack length can easily be observed on the surface. In other materials, like MDF, special

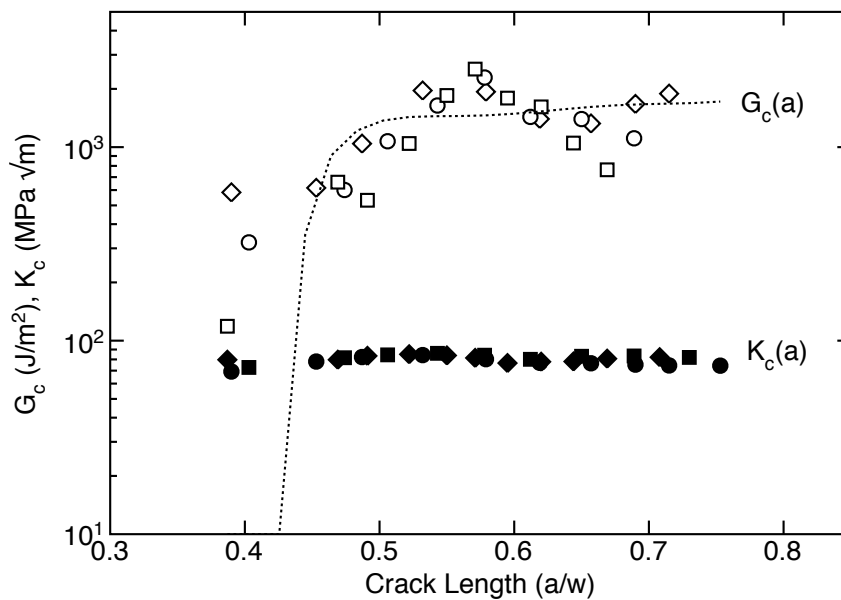


Figure 9: Experimental results for neat PSF crack propagation analyzed three different ways. The open symbols found toughness by discrete calculation of energy for each increment of crack growth using Eq. (1). The filled symbols found critical stress intensity factor using Eq. (6). The dotted line used fit curves for $P(a)$ and $C(a)$ and Eq. (3).

methods are required. The DIC method used here works well for relative crack length, Δa , needed for Eqs. (1) to (3), but not for absolute crack length.

Whether or not a material that unloads to the origin can additionally be analyzed for stress intensity factor using methods in ASTM E399, depends on how the compliance depends on crack length. For ASTM E399 to work, the crack propagation must be self-similar including self-similar crack tip stress states. Fracture process zones, such as those resulting from fiber bridging, invalidate the self similar nature of crack propagation. One way to test for self-similar crack growth is to measure compliance as a function of crack length and compare to ASTM E399 $Y(a/W)$ calibration functions using Eq. (9). Figure 11 shows the result of such a comparison for unidirectional carbon fiber/PSF composites, neat PSF, and Corian[®] sheet product. To facilitate comparison, the experimental results for compliance (left side of Eq. (9)) and the calibration function (right side of Eq. (9)) were both normalized to their value at $a/W = 0.6$. The compliance calibration curves for neat PSF and Corian[®] sheet product were close to the theoretical calibration curve (dashed curve in Fig. 11). This finding confirms these specimens could be analyzed using ASTM E399, which is consistent with the experimental results. The compliance calibration curve for unidirectional carbon fiber/PSF, however, differs significantly from the theoretical curve. This discrepancy was caused by the fiber bridging and confirms the unidirectional composite could not be analyzed by ASTM E399. It could, however, be analyzed by methods that directly measure energy or by methods that use the observed $C(a)$ rather than some implicitly assumed dependence of compliance on crack length.

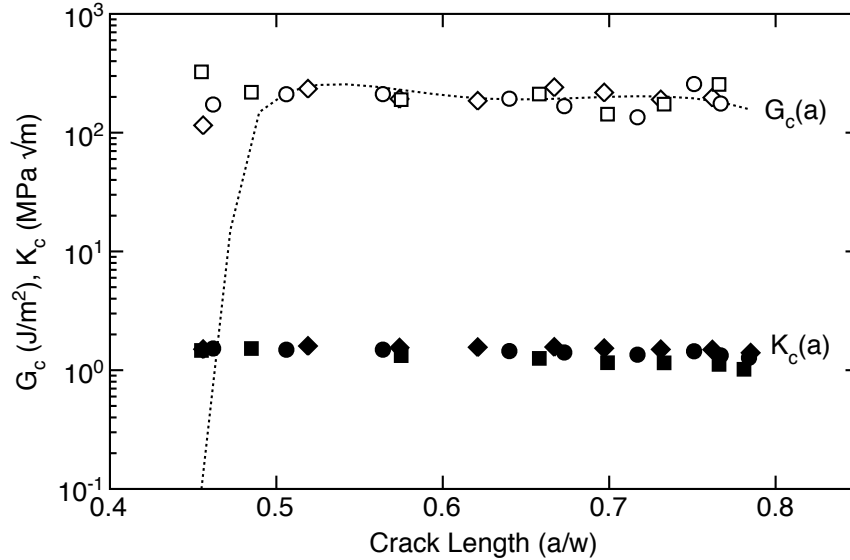


Figure 10: Experimental results for Corian® sheet product crack propagation analyzed three different ways. The open symbols found toughness by discrete calculation of energy for each increment of crack growth using Eq. (1). The filled symbols found critical stress intensity factor using Eq. (6). The dotted line used fit curves for $P(a)$ and $C(a)$ and Eq. (3).

When a material can be analyzed by ASTM E399, the analysis requires experiment results for load, P_i , and *absolute* crack length, a_i (see Eq. (6)). Since DIC methods that record only relative crack growth, Δa , would not be sufficient for finding absolute crack length, no material can be analyzed for stress intensity factor unless there is a clear way to record absolute crack length. Note that ASTM E399 is not a crack propagation experiment. The standard practice is to record only the initial load to cause the initial machined-in crack (of known length) to propagate. This approach avoids the need to measure the length of a propagating crack, but it does not provide enough information to determine if ASTM E399 can even be used. As discussed above, the experiment required to demonstrate self-similar crack propagation is to measure compliance as a function of crack length and compare it to the theoretical compliance calibration curve (*e.g.*, Fig. 11). This experiment can only be done if the standard ASTM E399 experiments are supplemented with additional experiments including crack propagation. Without these supplemental experiments, it is impossible to assert that ASTM E399 is valid for a given composite material.

If the first test reveals that the unloading curve does not return to the origin, the next task is to determine the reason for the residual displacement. The possibility of residual stresses changing the origin can be determined by inspection of the two fractured halves of the specimen. As long as they do not have residual stress-induced curvatures that were not present in the intact specimen, a residual stress cause can be eliminated [8]. Note that residual stresses may still be present and may influence fracture [10], but without macroscopic curvature in the separated pieces, the residual stresses will not cause residual displacements upon unloading.

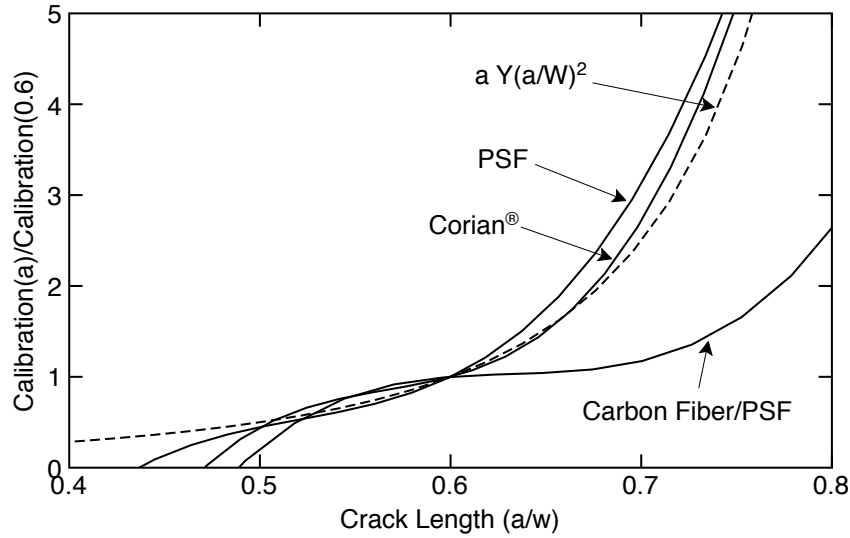


Figure 11: The compliance calibration function in Eq. (9) measured experimentally for PSF, Corian[®] sheet product and carbon fiber / PSF unidirectional composite. The dashed curve is the ASTM E399 theoretical result for $Y(a/W)$ for a compact tension specimen (see Eq. (5)) substituted into the right side of Eq. (9). All curves were normalized to their value at $a/W = 0.6$.

The remaining two causes for residual displacements are inelasticities (*e.g.*, plasticity) or crack-plane interferences (*e.g.*, pulled out fibers that cannot be pushed back in by unloading). These two effects can be separated by the described experiment of removing the crack process zone prior to unloading [3]. If this experiment still does not return to the origin, the material will require further work to analyze the inelastic effects. If this experiment does return to the origin, the material can only be analyzed by Eq. (2). The key experimental results are load, P_i , displacement, u_i , and relative crack growth, Δa , during cracking propagation. These results need to be determined during continuous loading because any unloading may alter the fracture properties due to crack-plane interference effects.

Of the materials studied here, unidirectional carbon fiber/PSF composites, neat PSF, and Corian[®] sheet product all passed the first test, *i.e.*, unloading curves returned close to the origin. Thus all these materials could be analyzed by energy methods in Eq. (1) to (3). The compliance calibration experiments revealed that unidirectional carbon fiber/PSF composites could not be analyzed by ASTM E399 due to fiber bridging effects. In contrast, both the homogeneous material (neat PSF) and the particulate-filled polymer (Corian[®] sheet product) did demonstrate self-similar crack propagation (see Fig. 11). Thus, these materials, and only these materials, could be analyzed by ASTM E399.

The MDF panels, however, did not return to the origin. By using the key experiment to remove the crack process zone, we found that unloading then did return close to the origin. We thus assumed that MDF fracture consisted primarily of elastic fracture processes, but that it exhibited crack-plane interference. MDF had the additional complication that it was difficult to measure crack growth. The DIC

methods made it possible to measure toughness using Eq. (2), provided the crack propagation experiments were done without any unloading.

There are prior results for MDF toughness, but each one has used methods that are claimed here to be invalid for characterization of MDF. Niemz *et al.* [11] followed ASTM E399. They reported $K_c = 1.81 \text{ MPa } \sqrt{\text{m}}$, which corresponds to a calculated $G_c = 1100 \text{ J/m}^2$ (assuming $E_{eff} = 3000 \text{ MPa}$), for MDF with a density of 0.710 g/cm^3 . This approach is invalid because MDF does not have self-similar crack propagation due to fiber bridging effects.

Morris *et al.* [12] measured toughness of MDF (density of 0.800 g/cm^3) as a function of relative humidity and found G_c from 5771 J/m^2 at 30% RH to 13075 J/m^2 at 90% RH. Unfortunately, the experimental details were provided in a report we did not have. It appears they took total area under a force-displacement curve divided by total fracture area. In other words, they equated a specific work of complete fracture to G_c . This approach approximately averages discrete G_c calculations as a function of crack length, such as the data in Fig. 6 for MDF, but averages all crack lengths instead of just the plateau region. A potential problem is that this approach will include short crack lengths, where the toughness is too low, and long crack lengths, where edge effects make the apparent toughness too high. The net result will be specimen-dependent results and an uncertain relation to the *true* material toughness.

The closest work to the present is crack propagation experiments in particle board by Ehart *et al.* [13]. Particle board differs from MDF, but still should be amenable to the methods in this paper. They calculated both total area (area ABCD in Fig. 3) and triangular area (area ABC in Fig. 3). As with MDF, they had problems observing crack growth and thus resorted to calculation of an effective crack length by normalization and comparison to an equivalent linear elastic material with no crack-tip process zone. They treated the full area as a “plastic energy” model and the triangular area as a “microcracking” model. They made no observation of which model was correct and had no experiment, such as the one used here, to identify crack-plane interference effects. Their “microcracking” model is probably the more realistic model, but because it relies on an effective crack length, it is only an effective toughness, rather than a *true* toughness.

We claim the new results here for lower density specimens (0.609 g/cm^3) of $G_c = 2650 \text{ J/m}^2$ and for the higher density specimens (0.769 g/cm^3) of $G_c = 5680 \text{ J/m}^2$ are the first *true* toughness results for MDF panels. Combining Eqs. (8) and (10) with $E_{eff} \leq 2500 \text{ MPa}$ and $\sigma_y \geq 20 \text{ MPa}$ [14], these two toughness correspond to $K_c = 2.57 \text{ MPa } \sqrt{\text{m}}$ and $K_c = 3.77 \text{ MPa } \sqrt{\text{m}}$ with thickness requirements for plane-strain conditions of $B \geq 41 \text{ mm}$ and $B \geq 88 \text{ mm}$ for the low and high density panels, respectively. The specimens thus did not produce plane-strain toughness results, but did show that MDF is very tough for a polymeric-based material. The key tasks for obtaining true toughness were to identify which part of the energy during crack propagation was actually related to crack growth and to use methods that allow accurate determination of the actual amount of crack growth. The methods used for MDF should be applicable

to numerous other materials where alternative elastic fracture mechanics methods may not be appropriate.

ACKNOWLEDGEMENTS

We thank David Kruse, from Flakeboard, for providing all the MDF panels and Milo Clauson, Oregon State University, for much help on mechanical testing and DIC methods.

REFERENCES

1. Kanninen, M. F., and Popelar, C. H., 1985. *Advanced Fracture Mechanics*. Oxford University Press, New York.
2. Annual Book of ASTM Standards 2005. "Standard Test Method for Plane-Strain Fracture Toughness of Metallic Materials," Vol 03.01, ASTM Designation: E399-90.
3. Atkins, A.G., Mai, Y-W, 1988. *Elastic and Plastic Fracture Mechanics: Metals Polymers, Composites, Biological materials*. John Wiley & Sons, Ellis Horwood Limited, Chichester, West Sussex, England.
4. Haygreen, J. G., and Bowyer, J. L., 1996. *Forest Products and Wood Science: An Introduction*. Iowa State University Press, Ames, Iowa, USA.
5. Nairn, J. A., 1987. "Transverse Fracture in Unidirectional Graphite/Polysulfone Composites," *J. Comp. Mat.*, 21: 798-808.
6. Bruck, H. A., McNeill, S. R., Sutton, M. A., and Peters, W. H. I., 1989. "Digital Image Correlation Using Newton-Raphson Method of Partial Differential Correction," *Experimental Mechanics*, 28: 261-267.
7. Muszyński, L., Lopez-Anido, R., and Shaler, S. M., 2000. "Image Correlation Analysis Applied to Measurement of Shear Strains in Laminated Composites," in: Proceedings of the SEM IX International Congress on Experimental Mechanics, Orlando, FL, June, 5-7, 2000, 163-166.
8. Nairn, J. A., 2006. "On the Calculation of Energy Release Rates for Cracked Laminates with Residual Stresses," *Int. J. Fract. Mech.*, 139: 267-293.
9. "UDEL® Polysulfone Design Guide," Solvay Advanced Polymers, Alpharetta Georgia, USA, 2002 (see <http://www.solvayadvancedpolymers.com/static/wma/pdf/4/0/6/UDG2004.pdf>).
10. Nairn, J. A. 1997. "Fracture Mechanics of Composites with Residual Thermal Stresses," *J. Appl. Mech.*, 64: 804-810.
11. Niemz, P., Diener, M., and Pöhler, E., 1997, "Untersuchungen zur Ermittlung der Bruchzähigkeit an MDF-Platten," *Holz als Roh- und Werkstoff*, 55: 327-330.
12. Morris, V.L., Hunt, D.G., and Adams, J.M. 1999. "The Effects of Experimental Parameters on the Fracture Energy of Wood-Based Panels," *Journal of the Institute of Wood Science*, 15(1): issue 85 Summer.
13. Ehart, R. J. A., Stanzl-Tschegg, and Tschegg, E. K., 1996. "Characterization of Crack Propagation in Particleboard," *Wood Sci. & Technology*, 30: 307-321.
14. Product Specifications, Flakeboard, Springfield, Oregon, USE (see <http://www.flakeboard.com>).